Long-Lived Fluorescence Probes for Studying Lipid Dynamics: A Review

Lesley Davenport[1,3] and Piotr Targowski[1,2]

A great many studies have focused on the heterogeneous packing of lipids in the bilayer matrix. However, less attention has been directed toward the temporal aspects of these lipid–lipid interactions. Studies of lipid packing fluctuations, or 'gel–fluid' exchange, using fluorescence probe methodologies have been limited. This limitation arises from the *submicrosecond* time scale over which the fluctuations are expected to occur. Traditionally, dynamic studies of lipid bilayers have been restricted to the nanosecond time regime, and the submicrosecond time 'window' has not been explored in any great depth by fluorescence methods, although persistent lipid dynamics has been evident. Probes with long fluorescence lifetimes (several hundred nanoseconds) have the potential to expand this important time 'window,' providing information on 'gel–fluid' exchange rates and insights into how important biological effectors such as proteins, cholesterol, and anesthetics affect or modulate these fluctuations. Using the long-lived fluorescence probe coronene, combined with time-resolved fluorescence methods geared toward microheterogeneity, we present a view of bilayer dynamics in an alternate time domain. Fluorescence probes are expected to inhabit an equilibrium between fluid and gel environments. Some probes remain in their respective environments throughout their excited-state lifetime, while others reside in surroundings that will change (i.e., 'melt'). Long-lived fluorescence membrane probes can provide direct estimates of submicrosecond lipid fluctuation or 'melt' rates. Simple Landau modeling leads to a *distribution* of 'melt' rates and provides an attractive alternative to a simpler *compartmental* model where a unique lipid fluctuation of gel–fluid exchange rate is measured. The *distribution* model is probe independent (defined by thermodynamic quantities) and can be applied generally to the rotational motions of fluorescence probes embedded in the lipid bilayer.

KEY WORDS: lipid dynamics; fluorescence probes; coronene; bilayers.

INTRODUCTION

Evidence for the existence of large-scale (micrometer) lateral phase separations or 'domains' in biological membranes [1,2] has arisen from many different studies, including direct visualization using electron [3] and/or video-enhanced [4,5] microscopies (which may be combined with particle tracking [6,7] or "laser tweezers"

[8]) or by elegant indirect spectroscopic methods (e.g., photobleaching techniques [9]). Such observations are perhaps not surprising in light of the very chemically heterogeneous composition of the cell membrane [10]. Interestingly, however, even for bilayers composed of one lipid type there is both experimental and theoretical evidence for so-called *dynamic* microheterogeneity [11]:

[1] Department of Chemistry, Brooklyn College of the City University of New York, Brooklyn, New York 11210.
[2] Permanent address: Institute of Physics, Nicolas Copernicus University, 87-100, Torun, Poland.
[3] To whom correspondence should be addressed.

[4] ABBREVIATIONS: DMPC, L-α-dimyristoylphosphatidylcholine; DPH, 1,6-diphenyl-1,3,5-hexatriene; DPPC, L-α-dipalmitoylphosphatidylcholine; DSC, differential scanning calorimetry; EA, fluorescence emission anisotropy; LUV, large unilamellar vesicles; SUV, small unilamellar vesicles; T_c, lipid phase transition temperature; *trans*-parinaric acid, all-*trans*-9,11,13,15-octadecatetraenoic acid.

strong lateral density fluctuations between neighboring lipid molecules on approaching the lipid melt transition result in the formation of lipid clusters composed of only a few tens of molecules which are not directly visible by microscopy tools. This view of the lipid matrix of the bilayer is thus one where ordered and disordered lipid clusters of variable size exist in dynamic equilibrium (*i.e.*, gel–fluid equilibrium) [12,13]. The terms 'gel' and 'fluid' are actually categories for a wide range of chain disorder, and this mixture is constantly changing with time. It is assumed that the size distribution of these clusters and their time-dependent alteration in size confer special properties on the lipid bilayer, and are fundamental to our understanding of the stability and so-called temporal persistence [1] of the 'quiltlike' phase-separated structures of biological membranes.

EVIDENCE FOR LIPID FLUCTUATIONS

Our current understanding of lipid dynamics has arisen largely from theoretical descriptions of lipid phase transitional behavior (for reviews see Refs. 14 and 15). In the region of the thermally induced pseudocritical lipid phase transition, enhanced thermodynamic fluctuations of the lipid-acyl chains occur and a microscopic equilibrium of 'gel' and 'fluid' lipid phases are expected to coexist. Two broad models have been proposed to explain such phenomena: phenomenological models (e.g., (long-range) Landau theory [16,17]) or statistical mechanical (microscopic) approaches (e.g., Monte Carlo simulations [18–20]). These studies suggest that thermodynamic fluctuations of lipid order, both *positional* (lateral motions of lipid molecules over the bilayer surface) and *conformational* (*gauche–trans* fatty-acyl links, perpendicular to the bilayer surface), may be responsible for many observable membrane-mediated events. Indeed, long-range thermodynamic fluctuations of lipid chain conformations are believed responsible for enhanced passive transport of Na^+ ions through the bilayer at the lipid melt transition temperature [21,22]. Other studies attribute bilayer compressibility [23] and increased lateral diffusion coefficients [24] to lipid structural fluctuations. Interestingly, recent studies by Goldstein and Leibler [25] suggest that water-mediated 'hydration repulsion' between interacting membranes may also be controlled by lipid fluctuation behavior. Ordered clusters are reported to form nucleation sites preceding gross lipid phase separations induced by cations [26] and may also play a significant role in bilayer destabilization processes required for membrane fusion [27]. Furthermore, it is not unreasonable to predict that

lipid fluctuations (*positional* or *conformational*) are involved in maintenance of fluidity gradients within lipid membranes [28–30]. This may play an important cellular role in transmembrane signaling mechanisms. These observations strongly suggest that studies of lipid bilayers must focus not only on the investigation of compositional lipid heterogeneity, but also on the associated kinetics and modulators (such as cholesterol and anesthetics) of these lipid exchange and/or fluctuation processes (i.e., dynamics controlling lipid heterogeneity).

EXPERIMENTAL INVESTIGATIONS OF LIPID FLUCTUATIONS

Physical methods required to detect all *dynamic* processes occurring within the bilayer must necessarily cover an extended time range. Studies by Holzwarth *et al.* [31] using iodine laser T-jump experiments revealed a broad temporal spectrum of relaxation events occurring in the lipid bilayer, ranging from 'fast' (picoseconds) *trans–gauche* conformational changes of the fatty-acyl chains, altered head-group and decreased monolayer interactions, and formation of gel or fluid lipid clusters, through to 'slow' (seconds) melting of the bilayer resulting in total disruption of lipid packing. As expected, there appears to be a gradual 'smearing' or redistribution of membrane order occurring at the phospholipid phase transition temperature T_c. Experimental studies of lipid order fluctuations have been somewhat limited, although a broad range of methodologies have been employed, including both macromolecular techniques (calorimetry [32–34], ultrasound [35–37]) and more localized probe techniques (NMR [38] and fluorescence [39–41]). From analogy with nematic crystals, relaxation times for lipid order fluctuations (gel–fluid exchange) are expected to be of the order of 10^{-7} s [42]. Dielectric measurements [43] and ultrasound studies [35–37] of lipid bilayers report submicrosecond relaxation times consistent with this expectation.

Time-dependent and steady-state fluorescence methods have proved vital for the investigation of the so-called *static* heterogeneity of lipid bilayers [44–47]. Probes used for these studies traditionally exhibit environmental spectral sensitivity and/or preferential partitioning, which allows quantitation of gel and fluid phases [48–50]. Alternatively, time-dependent fluorescence parameters may be assigned to a particular lipid phase [51–53] (in the case of mixed-lipid systems) or rotational environment [54,55] such as gel or fluid regions. These so-called *compartmental models* have proved attractive for visualization of lipid phases in bi-

layers where a measurable parameter can be linked to a particular environment [56,57].

From the anisotropic and/or restricted rotational diffusion of probes within membrane vesicles [44–46], the final anisotropy value r_∞ furnishes information on the structural (*conformational*) order of the acyl-chain region of the phospholipid bilayer [here the traditional order parameter is defined by $S = (r_\infty/r_0)^{1/2}$]. Interpretations for the origins of the limiting anisotropy term [46,54,55,57–61] have been the subject of many investigations and will not be discussed in detail here (see contribution by D. Toptygin and L. Brand in this issue).

Interestingly, there are discrepancies in structural order parameters (S) measured by different techniques for lipids in bilayers. Fluorescence [45,46,62–65] and Raman spectroscopies [66] report significantly higher lipid order than obtained via a number of magnetic resonance methods, such as ESR [67,68] and proton (^{1}H) [69] and deuterium (^{2}H) NMR [70,71]. Differences between these nanosecond-range and microsecond-range measurements may be taken as presumptive evidence for slow (submicrosecond) relaxations, and have been rationalized in terms of acyl-chain motion occurring at a rate of 10^{-7}–10^{-8} s [16,72,73].

USE OF FLUORESCENCE PROBES FOR STUDYING LIPID FLUCTUATIONS

Limitations of Short-Lived Fluorescence Probes

Studies of *submicrosecond* lipid fluctuations using traditional fluorescence probe methodologies have been limited. This limitation arises from the time scale over which the physical measurement occurs. In general, probes used for lipid heterogeneity studies (including the common 'disklike' [74,75] and 'rodlike' [51–55] molecules have relatively short ($\tau_{AV} < 20$ ns) fluorescence lifetimes when embedded in lipid bilayers. Under such conditions, submicrosecond lipid motions occur at frequencies lower than the fluorescence decay rate and a resultant averaged fluorescence signal is measured originating from the sampling of a distribution of lipid motions. Use of membrane probes with long-lived fluorescence decay rates (several tens of nanoseconds) can expand the 'time window' of observation and span this critical submicrosecond region. For conditions where the decay rate of the probe is comparable to the time scale of the lipid fluctuations, equilibrium is established and both time-resolved and steady-state fluorescence studies can provide convenient tools for investigation of lipid acyl-chain motions.

Studies Using Long-Lived Fluorescence Probes

Most previous lipid dynamic studies employing long-lived ($\tau_{AV} > 80$ ns in lipid systems) fluorescence probes have involved the use of *inter*molecular excimeric dyes (e.g., pyrene and its lipid analogs) to measure both short-range lateral diffusion coefficients [76,77] and molecular packing of the anisotropic lipid matrix [78,79]. However, recent hydrostatic pressure studies by Sassaroli *et al.* [80], using the *intra*molecular excimeric fluorescence probe di-(1'-pyrenedecanoyl)-phosphatidylcholine (dipy$_{10}$PC) in unsaturated lipid bilayer systems, suggest reduced volume fluctuations with increased pressure, resulting in hindrance of local rotational motions of the pyrene moieties and hence decreased intramolecular excimer formation. From these data, the authors speculate that such dynamic motions of the surrounding matrix lipids are expected to occur on a time scale of 10^{-7} s, somewhat longer than the lifetime of the probe.

Elegant studies by Ruggiero and Hudson [39] have interpreted the time-resolved fluorescence behavior of the relatively long-lived fatty-acyl chain analog *trans*-parinaric acid embedded in phosphatidylcholine LUV using a *dynamic* lipid fluctuation model. This unique molecule exhibits several desirable characteristics for studies of both *static* and *dynamic* lipid heterogeneity (discussed in detail elsewhere [54]). First, the all-*trans* isomer of the molecule partitions preferentially into gel-phase lipid and exhibits excitation spectral sensitivity to its environment. Furthermore, the fluorescence lifetime components for *trans*-parinaric acid can be assigned to gel ($\tau_G = 30$–50 ns) or fluid ($\tau_F \sim 3$ ns) phases of the bilayer. The amplitude of the long-lifetime component reveals a temperature dependence which is characteristic of critical phenomena. Estimates of the lifetime for lipid fluctuations are reported to range from about 10 ns to about 40 ns on approaching the lipid phase transition from temperatures greater than T_c and compare favorably with those determined by ultrasound studies (20–60 ns). The authors attribute differences in these lifetimes to distances over which the fluctuations are measured, i.e., microscopic versus macroscopic systems.

Steady-State Fluorescence Studies of Coronene-Labeled Lipid Bilayers

An alternative approach to the investigation of lipid fluctuations has focused on the rotational motions of a novel fluorescence probe, coronene, in gel-phase lipid bilayers [40,41]. This dye exhibits an average fluorescence lifetime of several hundreds of nanoseconds when embedded in lipid bilayers ($\tau_{AV} \sim 200$ ns). Under such
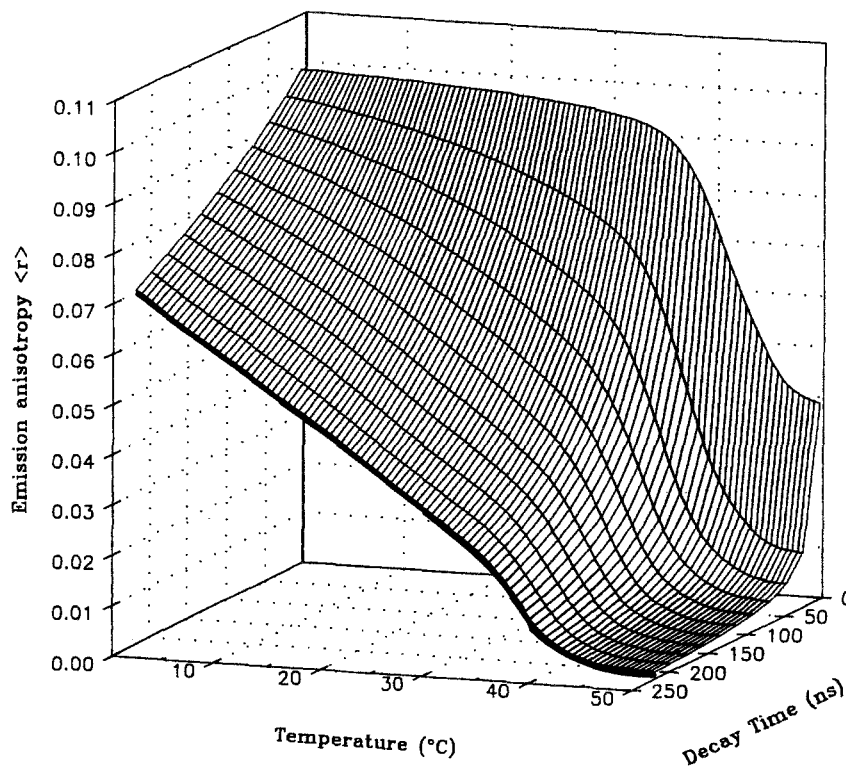
Steady state <r> as function of τ

Fig. 1. Surface plot of synthesized steady-state emission anisotropy as a function of temperature and lifetime of the fluorescence probe. From experimental time-resolved data for coronene-labeled DPPC SUV at 5°C ($\alpha_1 = 0.75$, $\tau_1 = 256$ ns; $\alpha_2 = 0.09$, $\tau_2 = 37$ ns; $\alpha_3 = 0.16$, $\tau_3 = 2$ ns) and the experimental $<r>(T)$ profile, an average lifetime and rotational correlation time (from the Perrin equation) is determined. The averaged fluorescence lifetime is then reduced from 200 to 5 ns, while the rotational parameters remain unchanged. The heavy line indicates the true experimentally obtained steady-state 'melt' curve for coronene, which is characteristically broad and shifted to colder temperatures.

conditions, targeting of slower (submicrosecond) lipid relaxation processes that occur well after the decay of most other fluorescence probes is possible. Unlike par-inaric acid, coronene appears to exhibit nonpreferential partitioning into coexisting gel or fluid lipid phases [40]. In addition, due to its disk-like shape (D_6h planar symmetry; $r_0 = 0.1$) [81], the polarized emissions of this molecule depend exclusively on out-of-plane probe motions ($<r_{op}>$). From steady-state emission anisotropy (EA) studies of this probe embedded in one-component lipid bilayers (e.g., DMPC or DPPC SUV), the appearance of fluctuation-induced rotations of coronene are evident in the gel phase of the membrane [40,41,82] at least 10° *below* the normally expected lipid transition temperature, as detected by differential scanning calorimetry (DSC) and EA versus temperature profiles for short-lived probes (e.g., DPH [83]). These experimental observations correlate well with theoretical modeling studies where fluid clusters are proposed to 'seed' at

temperatures where the bilayer is predominantly gel [84]. Figure 1 (heavy line) shows the observed shifted and broadened 'melt' transition profile obtained experimentally for coronene when embedded in DPPC SUV, which arises directly from the influence of submicrosecond lipid dynamics, detectable by virtue of the long fluorescence lifetime of the probe. This can be shown by modeling. From a knowledge of the time-dependent parameters measured for coronene in DPPC SUV (lifetime τ_{av} and rotational correlation times ϕ_{av}), it is possible through use of the Perrin equation [63] to construct steady-state fluorescence EA versus temperature profiles. Interestingly, as shown in Fig. 1, by reducing the average fluorescence lifetime from 200 ns to values more consistent with popular lipid dynamic probes (i.e., $\tau_{av} \sim$ 10 ns) while keeping the rotational motions for the probe unchanged (as influenced directly by the lipid environment), the melt transition profile for the lipid bilayers becomes better defined, and compares favorably with
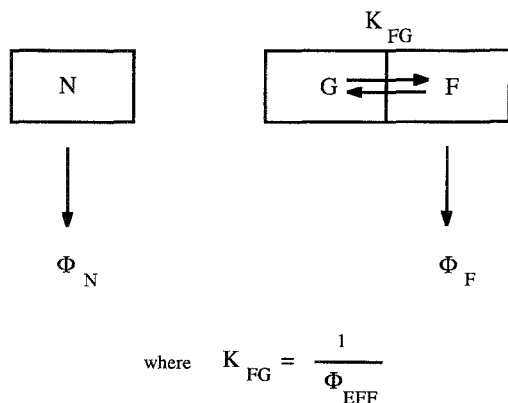
Fig. 2. Schematic representation of the *compartmental* model. Three lipid compartments are defined: a nonexchangeable fraction (N), where lipid does not melt appreciably on the microsecond time scale and included probes do not undergo any rotational motions until very close to T_c; the fluid (F) lipid (where $S \to 0$), where coronene molecules are free to rotate; the gel (G) region (where $S \to 1$). Regions F and G are in equilibrium on the submicrosecond time scale. An effective rotational time ϕ_{EFF} represents the rate of gel–fluid melting.

DPPC 'melt' transition profiles observed using DPH [83]. Hence, while the appearance of broadened and low-temperature-shifted lipid melt profiles have been observed from preferential lipid partitioning effects [85], in the case of long-lived fluorescence probes they can arise from the influence of submicrosecond lipid dynamics occurring in the gel phase. Indeed, such lipid melt curves are not specific to coronene; similar profiles have been observed for other long-lived fluorescence probes, e.g., pyrene derivatives ([86]). Short-lived fluorescence probes are not sensitive to submicrosecond lipid dynamics.

Theoretical Membrane Models for Interpretation of Time-Resolved Rotational Motions of Coronene

Polarized time-resolved data for coronene-labeled bilayer systems have provided information on fluctuation or gel–fluid lipid exchange rates. Two alternative membrane models have been employed for analyses of such complex experimental polarized multiexponential fluorescence decay profiles. In the first case, a simple *compartmental* model describing a unique gel–fluid exchange (fluctuation) rate between gel ($S = 1$) and fluid ($S = 0$) lipid phases may be adopted (Fig. 2). Alternatively, a *distributional* model has been developed. Here the membrane lipid exists as a distribution of lipid ordering ($0 \le S \le 1$), and lipid fluctuations between gel and fluid regions are now described by a *distribution* of lipid melt rates. Both models visualize the membrane as

a heterogeneously packed system with regions of coexisting gel ($S \to 1$) and fluid ($S \to 0$) lipid molecules.

Compartmental Model

In the case of a compartmental model, equilibrium populations of 'gel' (G) or 'fluid' (F) lipid phases are assumed to coexist (details of this model are discussed in Ref. 41 and more completely in Ref. 82). A third gel subfraction (N), not involved in the submicrosecond equilibrium, is included (Fig. 2), since a residual anisotropy term r_∞ (i.e., a nonexchangeable gel-lipid fraction) is evident from time-resolved anisotropy data of coronene at low temperatures. Coronene molecules included in this lipid compartment do not undergo rotational motions (ϕ_N) on this time scale. In contrast, coronene residing in fluid regions of the bilayer has rotational motions, $\phi_F \sim 2$ ns. Probes initially located in the exchangeable gel ($S = 1$) lipid regions (G) may rotate if the lipid goes through a local 'melting' process ($S = 0$). This melting process can thus be characterized by an effective rotational correlation time ϕ_{EFF} for the probe. The decay of the time-resolved emission anisotropy for coronene molecules distributed among the lipid compartments may be simply represented [41,82]:

$$r(t) = (\beta_F e^{-t/\phi_F} + \beta_G e^{-t/\phi_{EFF}} + \beta_N)e^{-t/\phi_N} \qquad (1)$$

where

$$\beta_F/r_0 = F/(G+F+N), \qquad \beta_G/r_0 = G/(G+F+N)$$

$$r_0 = \beta_F + \beta_G + \beta_N$$

It is pertinent to note that $\beta_G + \beta_N$ is equivalent to the limiting anisotropy term r_∞ obtained from time-resolved fluorescence EA profiles of probes with fluorescence lifetime shorter than those discussed here, e.g., DPH [54,63] and parinaric acid [39,55].

Values obtained for the fluctuation-induced effective rotational times ϕ_{EFF} of coronene as a function of increasing temperature range typically from 10 to 70 ns (depending on the temperature below T_c). These times are characteristic of equilibrium fluctuations or melt processes between gel and fluid regions in the bilayer, reflecting submicrosecond disordering of phospholipid packing; coronene probes originally embedded in the 'gel' regions can only rotate by going through a local 'melting' or fluctuation, and $\phi_{EFF} \equiv 1/K_{FG}$. Values of measured fluctuation lifetimes determined by this method show excellent correspondence with those reported by other methods, e.g., parinaric acid and ultrasonic studies.
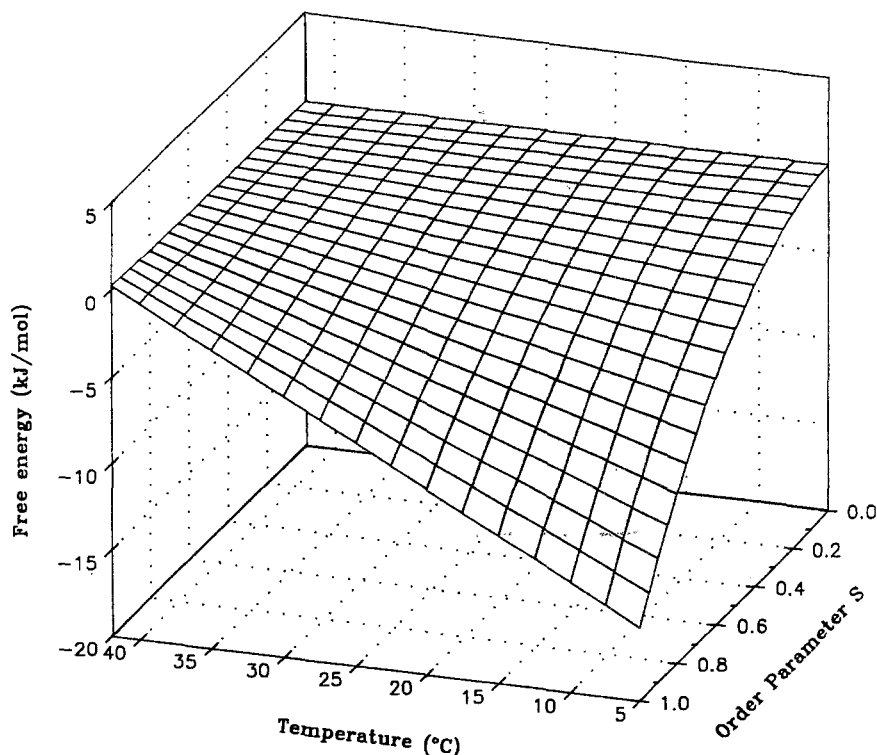
Fig. 3. Contour plot of the free energy for DPPC (kJ/mol) determined from the Landau expansion, as a function of order parameter (from $0 \to 1$) and temperature up to T_c. The coefficients for the expansion were taken from ultrasound studies [36] for DPPC. Values used were $A_1 = 0$; $A_2 = a(T_c - T)$, where $a = 1.35$ kJ/K; $A_3 = 6.8$ kJ/mol; $A_4 = 10.1$ kJ/mol. The free energy difference between the fluid ($T_c = 41°C$) and gel phase represents the activation energy of melting.

Distributional Model

An alternative model invokes a *distribution* of 'gel–fluid' exchange or fluctuation rates. Unlike the *compartmental model*, where lipids are characterized as gel ($S = 1$) or fluid ($S = 0$), here a continuum between these two extreme states of lipid order is envisaged resulting in a distribution of lipid order parameters (which is temperature dependent). Consequently a corresponding distribution of lipid melting rates $d(S,T)$ rather than a discrete (K_{FG}) gel–fluid melt rate is expected. Accordingly, discrete boundaries between 'gel' and 'fluid' are less well defined [87] and the bilayer exists as a dynamic unit with lipid phases of more ($S \to 1$) or less ($S \to 0$) well defined order.

This model (discussed in detail elsewhere [41,82]) is derived (based on reviews by Jähnig [16]) from Landau theory (which describes long-range phase transitional behavior) and attempts to provide an alternative expression for the time-resolved fluorescence EA decay function $r(t)$ of probes in lipid bilayers by including known thermodynamic parameters for the lipid system of interest.

The free energy F of the system at equilibrium can be determined explicitly using the fourth-order expansion of the Landau expression in powers of the *conformational* order parameter ($S = N^{-1} \Sigma_N S_n$, where n is the orientation of lipid segment n, and N is the total number of segments along the fatty-acyl chain):

$$F = -A_1 S + \frac{1}{2}A_2 S^2 - \frac{1}{3}A_3 S^3 + \frac{1}{4}A_4 S^4 ... \qquad (2)$$

The coefficients A_n of the free energy expansion are derived directly from measurable thermodynamic quantities, and have been determined explicitly from ultrasonic studies for a number of lipid systems [35–37]. Figure 3 shows a contour plot for such a free energy expansion for DPPC SUV as a function of both temperature (up to the main phase transition temperature T_c) and the *conformational* order parameter ($S = 0 \to 1$).

For gel-like lipid to effectively 'melt,' an activation energy proportional to the difference in free energy between the fluid [$F(S,T_c)$] and more ordered phase [$F(S,T)$] is required. The curves of Fig. 3 thus serve to quantify the energy penalty for chain disordering below
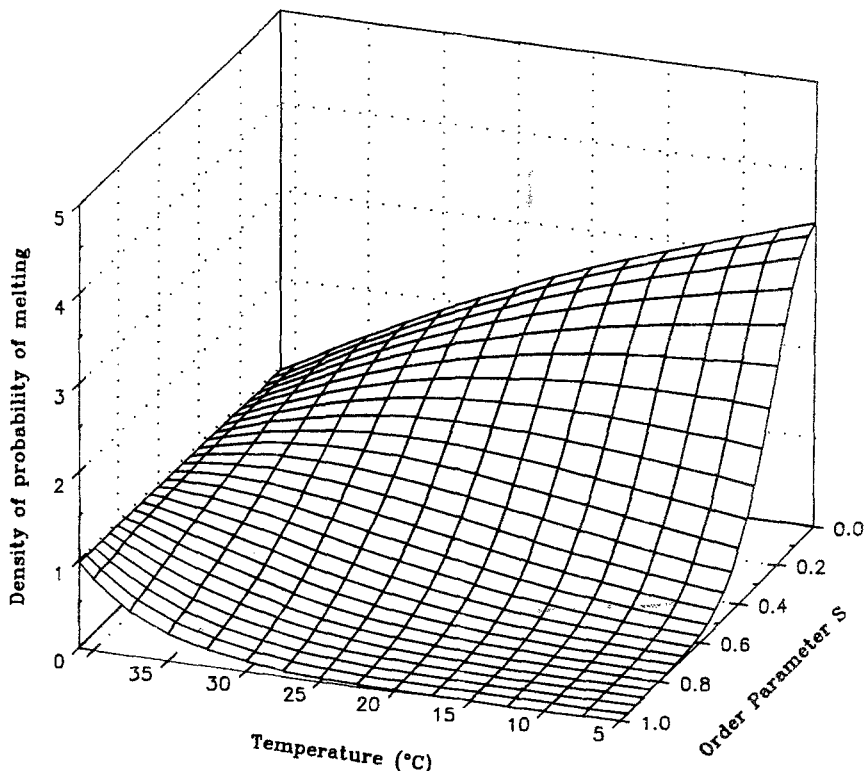
Fig. 4. Contour plot of the density of the melting probability $P(S,T)$ as a function of the order parameter and temperature. The probability of a lipid molecule melting with a given order parameter S at a particular temperature T is thus $P(S,T)dS$.

T_c for all possible existing order parameters in the range $S = 0 \rightarrow 1$:

$$E_{ACT}(S,T) = F(S,T_c) - F(S,T) \qquad (3)$$

At low temperatures, where bilayer systems are more ordered ($S \rightarrow 1$) and the differences in the free energy states are very large, the probability $P(S,T)$ of achieving the required E_{ACT} for melting will be more differentiated (Fig. 4) and low for the majority of lipids:

$$P(S,T) = (e^{-E_{ACT}(S,T)/RT}/(\int_{0\rightarrow 1}e^{-E_{ACT}(S,T)/RT}ds) \qquad (4)$$

In addition, an effective rotational rate $d(S,T)$ for a fluorescence probe embedded in the lipid may also be estimated from the activation energy barrier $E_{ACT}(S,T)$ which must be exceeded in order for lipid melting, and hence probe rotation, to occur. Since a distribution of order parameters exists for the lipids, a corresponding distribution of effective rotational rates is expected. Thus the activation energy E_{ACT} required for lipid 'melting' links both dynamic spectroscopic (local) parameters with static thermodynamic (global) parameters:

$$d(S,T) = d_\infty(T)e^{-\gamma E_{ACT}(S,T)/RT} \qquad (5)$$

γ defines a multiple of the activation energy barrier which must be overcome and thus represents the critical number of lipid molecules which must achieve 'disorder' simultaneously in order to permit probe rotation. This *gating factor* γ, as such, is indicative of a cooperative unit size of surrounding lipid which influences the rate of rotations of the included fluorescence probe molecule.

Combining these effective rotational rates [where $d(S,T) = 1/\phi(S,T)$] of the fluorescence probe with the probability $P(S,T)$ of a lipid melting through the activation energy $[(E_{ACT}(S,T)]$ term, we can express the time-resolved EA decay profile [82]:

$$r(t) = r_0\int_{0\rightarrow 1}P(S,T)e^{-d(S,T)t}dS \qquad (6)$$

Analysis of time-resolved EA decay profiles for coronene imbedded in DPPC SUV according to this model provided estimates for two variables, γ and the limiting diffusion rate [frequency factor; $d_\infty(T) = d(S = 0,T)$; see Eq. (5)]. Values obtained for the 'gating' factor γ ranged (nonlinearly) from 10 ± 20 at $20°C$ to 6 ± 1 at $35°C$, whereas $(d_\infty)^{-1}$ decreased linearly from 90 ± 20 ns at $20°C$, tending toward very fast subnanosecond rotational times at T_c [82].
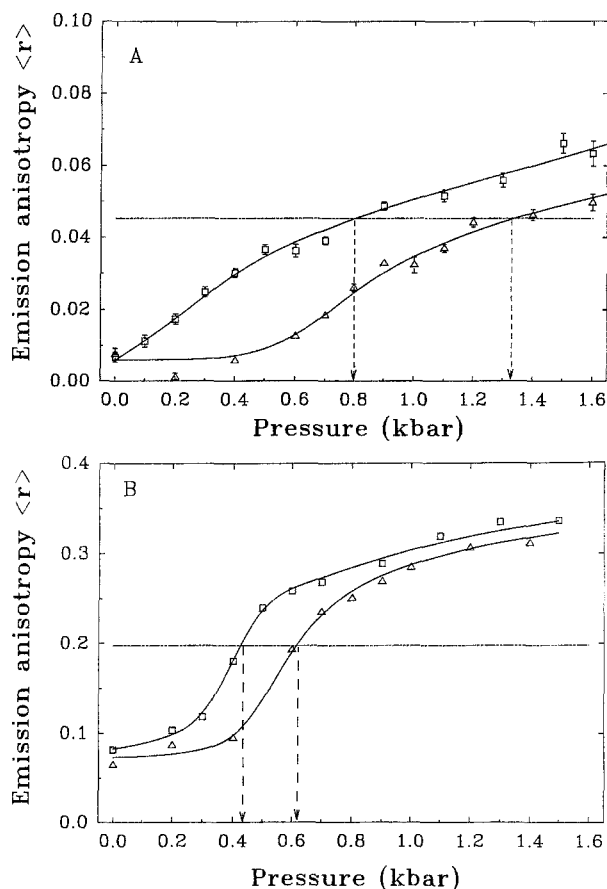
Fig. 5. Steady-state emission anisotropy as a function of increasing hydrostatic pressure for (A) coronene and (B) DPH-labeled DPPC SUV. Values of EA were corrected for scatter or birefringence artifacts as discussed elsewhere [102]. Excitation was achieved at 340 and 360 nm, respectively, and the wavelengths of observation were 448 and 430 nm, respectively. The two temperatures shown here are (△-△) 53.5°C and (□-□) 43.5°C. The $P_{1/2}$ values are indicated by arrows.

Lipid Fluctuations in Gel-Phase Bilayers as Revealed by Coronene Fluorescence

Analysis of time-resolved polarized data, either via the *compartmental* or *distributional* model, reveals that submicrosecond fluctuation-induced probe rotations [ϕ_{EFF} or $\phi(S,T)$, respectively] are evident at temperatures well below T_c. From the overall head-group surface area for DPPC of 50 ± 2 Å² (below the phase transition) [83] and the dimensions of the coronene carbon skeleton, values of γ suggest that several lipid shells surrounding the probe are involved in the lipid chain disordering process, with estimated lipid 'cluster' sizes on the order of 25–40 Å in diameter. Cluster sizes ranging from 20 to 50 Å were recently estimated by Parasassi *et al.* [88], using preferential partitioning in a two-component lipid system, of the environmentally sensitive fluorescence mem-

brane probe Laurdan (see contribution by T. Parassasi and E. Gratton in this issue). Estimated sizes for lipid clusters determined from fluorescence spectroscopic measurements are significantly smaller than those previously reported for corresponding lipid systems determined using Monte Carlo simulations [11] or by thermodynamic analyses of experimental heat capacity curves. Indeed, Biltonen and co-workers [32,34] report average cluster sizes of several hundreds of lipid molecules in the region approaching the melt transition. It is of importance to emphasize that values of γ reported here represent only those neighboring lipids that affect the rotations of coronene. In contrast to cluster sizes defined by DSC studies, here the cooperative unit is defined by a multiple of the activation energy barrier required for lipid melting and therefore probe rotation.

Direct experimental evidence for the formation of large clusters during the lipid bilayer melting transition has come from electron-microscopic investigations of isolated two-component lipid phosphatidylcholine vesicles [89], although clusters in single-component lipid vesicles have not been directly observed, except in the presence of Ca^{2+} [90] (which induces 'gross' phase separations [26]) or by elegant HPLC dimerization studies [91]. Recent ultrasound studies [37] suggest that cluster sizes are intimately associated with the radius of vesicle curvature. In this comparative study, SUV had smaller cluster sizes (85 lipids for DMPC SUV) over the several hundred lipid molecules estimated for corresponding LUV.

The effects of applied hydrostatic pressure (0–1.2 kbar) on submicrosecond lipid motions in lipid bilayers using coronene [92] have also been examined. Pressure provides an alternative independent variable resulting exclusively in volume changes for a constant temperature. Hence resolution of lipid packing and density effects from those directly attributable to thermal change is possible. In addition, pressure provides an important mechanism for biological adaptation to the environment, resulting in altered lipid composition and changed phase separations or domain architecture in the biological membrane. By including a pressure-dependent term in the free energy expansion (i.e., $A_1 \neq 0$ in Eq. (2) [16]) while keeping all other inherent thermodynamic parameters fixed for the lipid system under investigation, pressure-induced steady-state EA melt curves for DPPC SUV have been successfully reconstructed using previously determined gate factors γ and limiting diffusion constants obtained from temperature-dependent experiments ($P = 0$). Figure 5 shows typical experimentally obtained EA versus pressure profiles for coronene and DPH-labeled DPPC SUV at 43.5 and 53.5°C. Interest-

ingly, the pressure-induced phase transitions as detected by increased EA values for coronene are shifted to higher pressure values ($P_{1/2}$ = 0.80 and 1.33 kbar, respectively) than for corresponding DPH-labeled samples ($P_{1/2}$ = 0.43 and 0.62 kbar, respectively). It appears, as might be predicted [80], that a greater applied pressure is required to restrict the rotational motions of coronene by hindering or 'freezing out' slow (submicrosecond) lipid motions.

FUTURE DIRECTIONS

Within the framework of the dynamic heterogeneous membrane models discussed here, we can now proceed to perturb the partitioning of a fluorescence marker between gel and fluid lipid regions by introducing intrinsic (cholesterol, peptide, and proteins) and/or extrinsic (Ca^{2+}, anesthetics) modulators into the system (i.e., effectively shift the melt equilibrium). The dynamics of such systems are not well understood [93,94] and experimental investigations are limited [37,95–97]. Nevertheless, it is important to understand them, since lipid fluctuations are reported to play important roles in the controlled functioning of membrane enzymes [98] and photosynthetic reaction centers [99]. Fluorescence methodologies using long-lived probes can provide important insights into such dynamics. Indeed, recent studies by Montejo et al. [100] have examined submicrosecond protein conformational changes using 1-methylpyrene conjugates of human fibrinogen. Preliminary studies of melittin-containing lipid bilayers using coronene or a coronene–phospholipid adduct (Cor-PC; τ_{AV} ~ 120 ns [101]) (where the fluorescent reporter is located at a fixed depth in the bilayer) revealed increased steady-state EA values at temperatures below T_c, suggesting a lipid ordering effect in the presence of peptide (1:50 peptide-to-lipid molar ratio). In contrast, DPH-labeled systems showed no significant alteration in steady-state EA values with introduction of melittin into the bilayer [86]. It is apparent that long-lived fluorescence probes provide sensitivity to lipid–peptide effects occurring on a 'slow' time scale. Future time-resolved polarized studies will provide interesting insights into *submicrosecond* gel–fluid lipid exchange rates as affected by the presence of peptide.

ACKNOWLEDGMENTS

REFERENCES

1. M. Edidin (1992) *Trends Cell Biol.* **2**, 376–380.
2. K. Jacobson and W. Vaz (1992) *Comm. Mol. Cell. Biophys.* **8**, 1–114.
3. D. S. Friend and D. W. Fawcett (1974) *J. Cell Biol.* **63**, 641–664.
4. K. Florine-Casteel, J. J. LeMastes, and B. Herman (1991) *FASEB J.* **5**, 2078–2084.
5. L. Finzi, C. Bustamante, G. Garab, and C. B. Juang (1989) *Proc. Natl. Acad. Sci. USA* **86**, 8748–8752.
6. G. M. Lee, A. Ishihara, and K. A. Jacobson (1991) *Proc. Natl. Acad. Sci. USA* **88**, 6274–6278.
7. R. Ghosh and W. W. Webb (1990) *Biophys. J.* **57**, 286a.
8. S. C. Juo and M. P. Sheetz (1992) *Trends Cell Biol.* **2**, 116–117.
9. A. Chakrabart, J. Matko, N. A. Rahman, B. G. Barisas, and M. Edidin (1992) *Biochemistry* **31**, 7182–7189.
10. G. Daum (1985) *Biochim. Biophys. Acta* **822**, 1–42.
11. J. H. Ipsen, J. Jorgensen, and O. G. Mouritsen (1990) *Biophys. J.* **58**, 1099–1107.
12. O. G. Mouritsen (1983) *Biochim. Biophys. Acta* **731**, 217–221.
13. M. L. Johnson, W. W. van Osdol, and R. L. Biltonen (1986) Volume-perturbation kinetic calorimeter, in *Methods in Enzymology*, Vol. **130**, Academic Press, pp. 534–551.
14. G. Cevc and D. Marsh (1987) *Phospholipid Bilayers. Physical Principles and Models*, Wiley-Interscience, New York.
15. O. G. Mouritsen (1984) *Phase Transitions and Critical Phenomena*, Springer-Verlag, New York.
16. F. Jähnig (1981) *Biophys. J.* **36**, 329–345.
17. F. Jähnig (1981) *Biophys. J.* **36**, 347–357.
18. S. Doniach (1978) *J. Chem. Phys.* **68**, 4912–4916.
19. O. G. Mouritsen, A. Boothroyd, R. Harris, N. Jan, T. Lookman, L. MacDonald, D. A. Pink, and M. J. Zuckermann (1983) *J. Chem. Phys.* **79**, 2027–2041.
20. M. J. Zuckerman, D. A. Pink, M. Costas, and B. C. Sanctuary (1982) *J. Chem. Phys.* **76**, 4206–4216.
21. J. F. Nagle, and J. L. Scott, Jr. (1978) *Biochim. Biophys. Acta* **513**, 236–243.
22. M. I. Kanehisa and T. Y. Tsong (1978) *J. Am. Chem. Soc.* **100**, 424–432.
23. O. Albrecht, H. Gruler, and E. Sackman (1978) *J. Physiol.* (Paris) **39**, 301–313.
24. E. S. Wu, K. Jacobson, and D. Papahadjopoulos (1977) *Biochemistry* **16**, 3936–3941.
25. R. E. Goldstein and S. Leibler (1989) *Phys. Rev. A* **40**, 1025–1035.
26. D. Hoekstra (1982) *Biochemistry* **21**, 1055–1061.
27. D. Hoekstra (1982) *Biochemistry* **21**, 2833–2840.
28. E. Blatt and W. H. Sawyer (1985) *Biochim. Biophys. Acta* **822**, 43–62.
29. D. Marsh (1981) *Mol. Biol. Biochem. Biophys.* **31**, 51–142.

30. J. R. Wardlaw, W. H. Sawyer, and K. Ghiggino (1987) *FEBS Lett.* **223**, 20–24.
31. J. F. Holzwarth, V. Eck, and A. Genz (1985) in P. M. Bayley and R. E. Dale (Eds.), *Spectroscopy and the Dynamics of Molecular Biological Systems*, Academic Press, London, pp. 351–377.
32. E. Freire and R. Biltonen (1978) *Biochim. Biophys. Acta* **514**, 54–68.
33. S. Imaizumi and C. W. Garland (1987) *J. Phys. Soc. Jpn.* **56**, 3887–3892.
34. R. Biltonen (1990) *J. Chem. Thermodynamics* **22**, 1–19.
35. S. Mikaku, A. Ikegami, and A. Sakanishi (1978) *Biophys. Chem.* **8**, 295–304.
36. S. Mitaku, T. Jippo, and R. Kataoka (1983) *Biophys. J.* **42**, 137–144.
37. B. Michels, N. Fazel, and R. Cerf (1989) *Eur. Biophys. J.* **17**, 187–190.
38. M. H. Hawton and J. W. Doane (1987) *Biophys. J.* **52**, 401–404.
39. A. Ruggiero and B. Hudson (1989) *Biophys. J.* **55**, 1111–1124.
40. L. Davenport, J. R. Knutson, and L. Brand (1989) *Subcell. Biochem.* **14**, 145–188.
41. L. Davenport, J. R. Knutson, and L. Brand (1988) in J. R. Lakowicz (Ed.), *Time-Resolved Laser Spectroscopy in Biochemistry*, Proceedings SPIE **909**, pp. 263–270.
42. P. G. deGennes (1974) *The Physics of Liquid Crystals*, Oxford University Press, London, Chapters 2–5.
43. U. Kaatze, R. Henze, and R. Pottel (1979) *Chem. Phys. Lipids* **25**, 149–177.
44. M. P. Andrich and J. M. Vanderkooi (1976) *Biochemistry* **15**, 1257–1261.
45. J. R. Lakowicz, F. G. Prendegast, and D. Hogan (1979) *Biochemistry* **18**, 508–519.
46. S. Kawato, K. Kinosita, Jr., and A. Ikegami (1977) *Biochemistry* **16**, 2319–2324.
47. S. Wang, J. M. Beechem, E. Gratton, and M. Glaser (1991) *Biochemistry* **30**, 5565–5572.
48. W. Stillwell, S. R. Wassall, A. C. Damaual, and W. D. Ehringer (1993) *Biochim. Biophys. Acta* **1146**, 136–144.
49. P. L. Chong (1988) *Biochemistry* **27**, 399–404.
50. C. R. Mateo, M. P. Lillo, J. Gonzalez-Rodriguez, and A. U. Acuna (1991) *Eur. Biophys. J.* **20**, 53–59.
51. B. R. Lentz, Y. Barenholz, and T. E. Thompson (1976) *Biochemistry* **15**, 4521–4528.
52. B. R. Lentz, Y. Barenholz, and T. E. Thompson (1976) *Biochemistry* **15**, 4529–4536.
53. R. D. Klausner, A. M. Kleinfeld, R. L. Hoover, and M. J. Karnovsky (1980) *J. Biol. Chem.* **255**, 1286–1295.
54. L. Davenport, J. Knutson, and L. Brand (1986) *Biochemistry* **25**, 1811–1816.
55. L. A. Sklar, B. S. Hudson, and R. D. Simoni (1977) *Biochemistry* **16**, 819–828.
56. G. L. Atkins (1969) in *Multicompartment Models in Biological Systems*, Methuen, London.
57. L. Davenport, J. R. Knutson, and L. Brand (1986) *Faraday Discuss. Chem. Soc.* **81**, 81–94.
58. G. Lipari and S. Szabo (1980) *Biophys. J.* **30**, 489–506.
59. C. Zannoni (1979) *Mol. Phys.* **38**, 1813–1837.
60. W. van der Meer, H. Pottel, W. Herreman, M. Ameloot, H. Hendrickx, and H. Schroder (1984) *Biophys. J.* **46**, 515–523.
61. D. Toptygin, J. Svobodova, I. Konopasek, and L. Brand (1992) *J. Chem. Phys.* **96**, 7919–7930.
62. P. K. Wolber and B. S. Hudson (1981) *Biochemistry* **20**, 2800–2808.
63. R. E. Dale, L. A. Chen, and L. Brand (1977) *J. Biol. Chem.* **252**, 7500–7510.
64. M. P. Heyn (1979) *FEBS Lett.* **108**, 359–364.
65. F. Jahnig (1979) *Proc. Natl. Acad. Sci. USA* **76**, 6361–6365.
66. R. Medelson, S. Sunder, and H. J. Berstein (1976) *Biochim. Biophys. Acta* **49**, 563–569.
67. W. L. Hubbell and H. M. McConnell (1968) *Proc. Natl. Acad. Sci. USA* **61**, 21–16.
68. P. Jost, A. S. Waggoner, and O. H. Griffith (1971) Spin-labelling and membrane structure, in L. I. Rothfield (Ed.), *Structure and Function of Biological Membranes*, Academic Press, New York, pp. 83–144.
69. C. H. A. Seiter and S. I. Chan (1973) *J. Am. Chem. Soc.* **95**, 7541–7553.
70. A. Seelig and J. Seelig (1974) *Biophys. Res. Commun.* **57**, 406–410.
71. G. W. Stockton, C. F. Polnaszek, A. P. Tulloch, F. Hasa, and I. C. P. Smith (1976) *Biochemistry* **15**, 954–966.
72. N. O. Peterson and S. I. Chan (1977) *Biochemistry* **16**, 2657–2667.
73. B. J. Gaffney and H. H. McConnell (1974) *J. Mag. Res.* **16**, 1–28.
74. J. Lakowicz and J. R. Knutson (1980) *Biochemistry* **19**, 905–911.
75. P. L. Chong, B. Wieb van der Meer, and T. E. Thompson (1985) *Biochim. Biophys. Acta* **813**, 253–265.
76. H. J. Galla and E. Sackmann (1974) *Biochim. Biophys. Acta* **339**, 103–115.
77. K. A. Zachariasse, W. Kuhnle, and A. Weller (1980) *Chem. Phys. Lett.* **73**, 6–11.
78. D. Tang and P. L. Chong (1992) *Biophys. J.* **63**, 903–910.
79. B. Wieb van der Meer, K. H. Cheng, and S.-Y. Chen (1990) *Biophys. J.* **58**, 1517–1526.
80. M. Sassaroli, M. Vauhkonen, P. Somerharju, and S. Scarlatta (1993) *Biophys. J.* **64**, 137–149.
81. V. H. Zimmerman and N. Joop (1961) *Z. Elektrochem.* **65**, 138–142.
82. L. Davenport and P. Targowski (1994) *Biochemistry*, submitted.
83. L. Davenport, R. E. Dale, R. H. Bisby, and R. B. Cundall (1985) *Biochemistry* **24**, 4097–4108.
84. O. G. Mouritsen and M. J. Zuckermann (1985) *Eur. J. Biophys.* **12**, 75–86.
85. K. R. Thulborn (1981) in G. Beddard and M. A. West (Eds.), *Fluorescent Probes*, Academic Press, pp. 113–141.
86. L. Davenport, J. Wang, and J. R. Knutson (1989) in A. Butterfield (Ed.), *Biological and Synthetic Membranes*, Alan R. Liss, New York, pp. 97–106.
87. W. L. C. Vaz, E. C. C. Melo, and T. E. Thompson (1989) *Biophys. J.* **56**, 869–876.
88. T. Parassasi, G. Ravagnan, R. M. Rusch, and E. Gratton (1993) *Photochem. Photobiol.* **57**, 403–410.
89. S. W. Hui (1981) *Biophys. J.* **34**, 383–395.
90. D. M. Haverstick and M. Glaser (1987) *Proc. Natl. Acad. Sci. USA* **84**, 4475–4479.
91. S. M. Krisovitch and S. L. Regen (1991) *J. Am. Chem. Soc.* **113**, 8175–8180.
92. L. Davenport and P. Targowski (1993) *Biophys. J.* **34**, A75.
93. M. M. Sperotto and O. G. Mouritsen (1993) *Eur. Biophys. J.* **22**, 323–328.
94. J. H. Ipsen, O. G. Mouritsen, and M. Bloom (1990) *Biophys. J.* **57**, 405–412.
95. A. Genz, J. F. Holzwarth, and T. Y. Tsong (1986) *Biophys. J.* **50**, 1043–1051.
96. Z.-Y. Peng, N. Tjandra, V. Simplacenu, and C. Ho (1989) *Biophys. J.* **56**, 877–885.
97. W. W. van Osdol, Q. Ye, M. L. Johnson, and R. L. Biltonen (1992) *Biophys. J.* **63**, 1011–1017.
98. M. Menashe, G. Romero, R. L. Biltonen, and D. Lichtenberg (1986) *J. Biol. Chem.* **261**, 5328–5333.
99. F. Drepper, I. Carlberg, B. Anderson, and W. Haehnel (1993) *Biochemistry* **32**, 11915–11922.
100. J. M. Montejo, K. R. Naqui, M. P. Lillo, J. Gonzalez-Rodriguez, and A. U. Acuna (1992) *Biochemistry* **31**, 7580–7586.
101. B. Shen, J. Lobo, P. Targowski, and L. Davenport (1994) *Biophys. J.* **66**, A58.
102. A. A. Paladini and G. Weber (1981) *Rev. Sci. Instrum.* **52**, 419–429.